

DEVELOPMENT STUDIES FOR THE OPAL END CAP ELECTROMAGNETIC CALORIMETER USING VACUUM PHOTO TRIODE INSTRUMENTED LEADGLASS

M. AKRAWY ²⁾, G.T.J. ARNISON ³⁾, J.R. BATLEY ²⁾, K.W. BELL ³⁾, R.M. BROWN ³⁾, A.A. CARTER ²⁾, J.R. CARTER ¹⁾, W.M. EVANS ³⁾, N.I. GEDDES ³⁾, C.N.P. GEE ³⁾, W.R. GIBSON ²⁾, M.J. GOODRICK ¹⁾, P.W. JEFFREYS ³⁾, P. KYBERD ²⁾, G.N. PATRICK ³⁾, M.D. ROUSSEAU ^{3)†}, R.A. SANSUM ³⁾, B.J. SAUNDERS ³⁾, M. SPROSTON ³⁾ and C.P. WARD ¹⁾

¹⁾ *Cavendish Laboratory, University of Cambridge, Madingley Road, Cambridge, CB3 0HE, England*

²⁾ *Queen Mary and Westfield College, Department of Physics, Mile End Road, London, E1 4NS, England*

³⁾ *Rutherford Appleton Laboratory, Chilton, Didcot, Oxon, OX11 0QX, England*

Received 3 July 1989 and in revised form 23 November 1989

A description is given of the OPAL end cap electromagnetic calorimeters which consist of leadglass instrumented with vacuum photo triodes. Test results are presented showing linearity, energy and position resolution measured in an electron beam whilst the calorimeter is subject to magnetic fields up to 1.0 T. The response to hadrons is also discussed. Finally, radiation damage and recovery of the leadglass is reported.

1. Introduction

OPAL [1] is one of four experiments under preparation for the LEP e^+e^- collider at CERN. It is shown schematically in fig. 1. It is divided into a “barrel region” with various detectors arranged in concentric cylinders around the collision zone and two “end cap” regions which close the cylinders to complete the solid angle coverage. Electromagnetic calorimetry, a vital part of the detector, is used to detect and measure the energy and direction of photons and electrons and to provide fast trigger signals. This article is devoted to the end cap electromagnetic calorimeters. A cross-section through one of them is shown in fig. 2. It is a total absorption calorimeter, and consists of a matrix of leadglass assemblies located between the OPAL central drift chamber pressure vessel and the magnet iron pole pieces. Each end cap forms a 3.8 m diameter dome of leadglass counters covering the polar angular regions $10^\circ \leq \theta \leq 35^\circ$, where θ is the angle with respect to the beam line, and the whole azimuthal angle. The total solid angle covered by the end caps is 17%. The end cap electromagnetic calorimeters overlap with forward calorimeters [2] at small polar angles and with the barrel electromagnetic calorimeters [3] at large polar angles.

Fig. 3 shows a complete electromagnetic end cap (EMEC). It is made up from two halves, known as “Dees”, each consisting of 566 leadglass assemblies.

There are a total of 2264 for the entire EMEC detector. The lateral dimensions of the individual counters are $94 \times 94 \text{ mm}^2$, comparable to the lateral size of electromagnetic showers. The front face of each counter subtends an angle of approximately $2^\circ \times 2^\circ$ at the intersection region.

The EMECs are subject to the full axial magnetic field of the OPAL magnet. Initially this will be 0.4 T, possibly rising to 0.7 T if the aluminium coil is replaced with a superconducting one. The light within the leadglass is detected with novel devices which we have developed in conjunction with industry and designed to operate in intense axial magnetic fields. They are single stage photomultipliers or vacuum photo triodes [4] (VPTs).

Thin, high gas gain wire chambers [5] are mounted between the OPAL central detector pressure vessel and the leadglass to “presample” the electromagnetic showers, making it possible to correct, on a particle-by-particle basis, for energy deposited in the material in front of the calorimeter.

The EMEC calorimeter design aims are:

- excellent energy linearity and intrinsic resolution;
- good spatial resolution ($\leq 1 \text{ cm}$);
- good gain stability plus accurate gain monitoring;
- hermiticity;
- good electron–hadron identification;
- affordable price;
- able to operate in a high magnetic field.

In addition the EMEC calorimeters must be reliable and robust.

† Deceased.

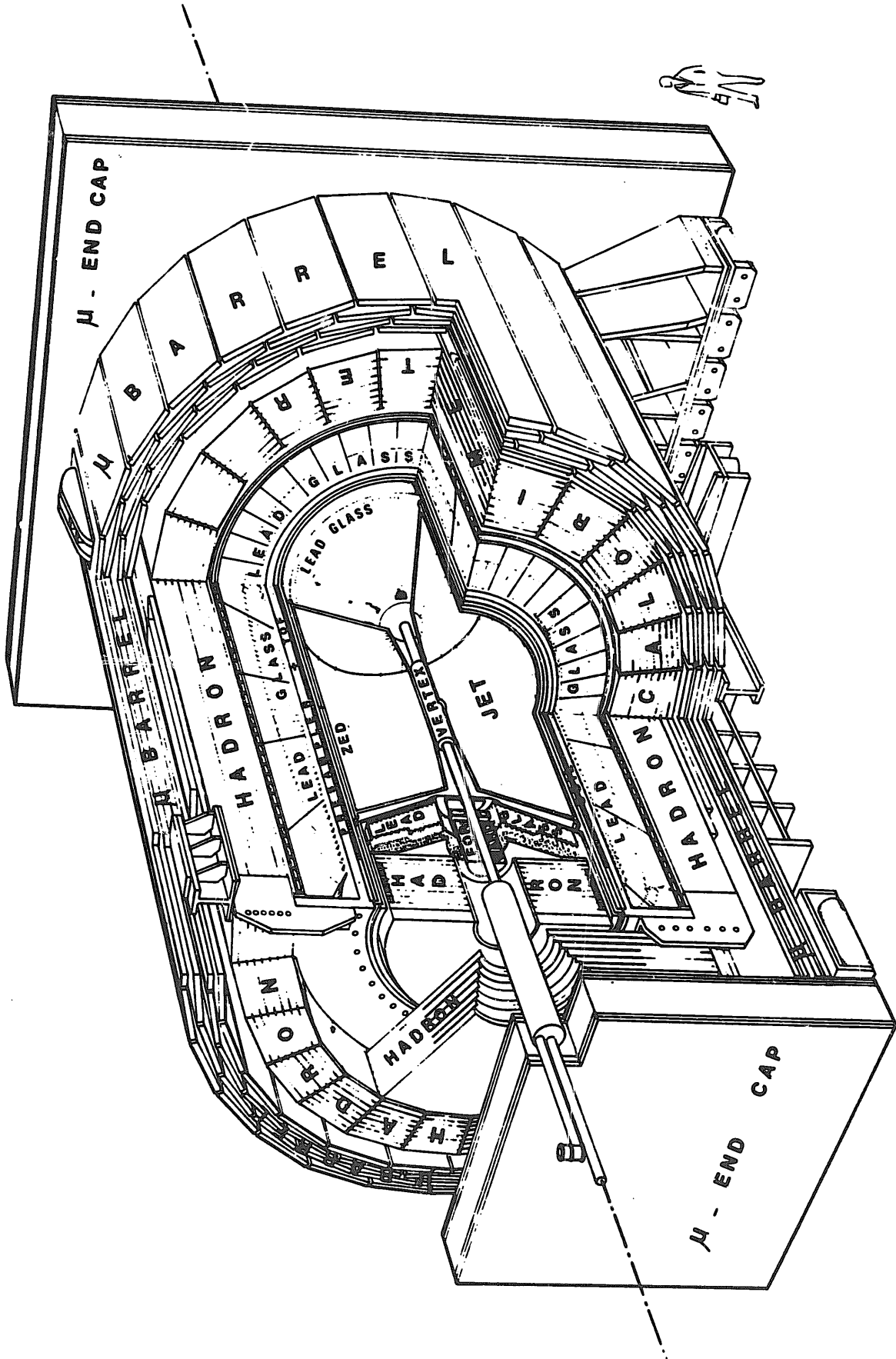


Fig. 1. Schematic view of the OPAL experiment.

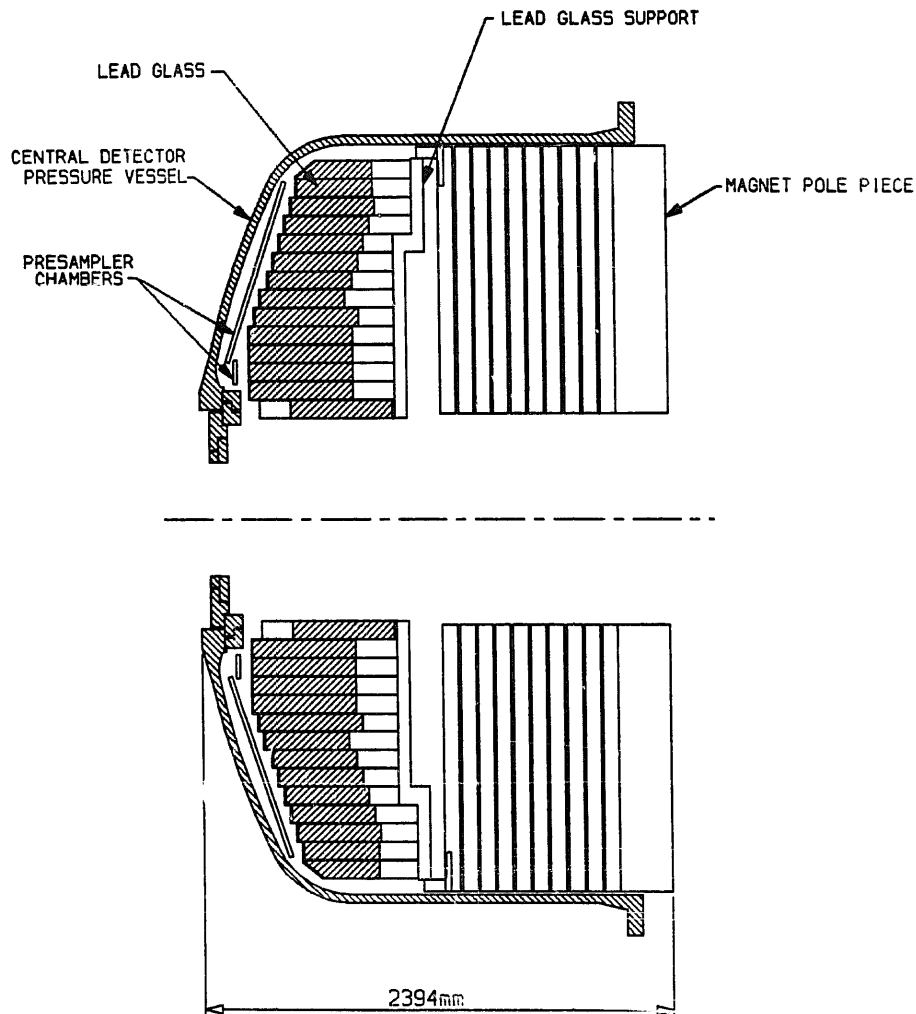


Fig. 2. Cross section through OPAL end cap showing the different lengths of leadglass blocks.

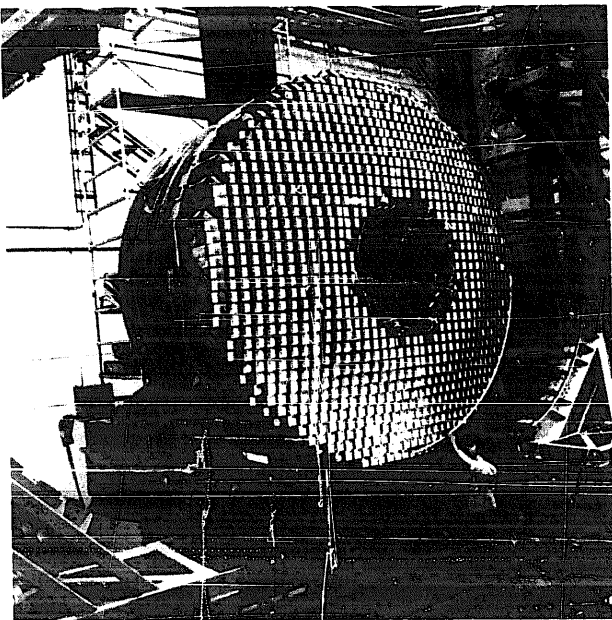


Fig. 3. A complete OPAL end cap electromagnetic calorimeter consisting of two Dees, mounted on the OPAL magnet pole piece.

This paper describes the detailed design of the EMEC assemblies, and reports a series of test beam studies to measure their performance (a forthcoming paper [6], hereafter referred to as OPAL 2, will address the construction, calibration and operation of the complete EMEC apparatus).

Section 2 describes in detail the EMEC assembly design, section 3 covers the experimental arrangements used in the test beams, section 4 summarises the beam test results for single assemblies operated in an axial magnetic field, section 5 reports the test beam results for an array of assemblies and section 6 discusses the effect of radiation on the leadglass.

2. EMEC assembly design and description

Leadglass has been chosen for the EMEC calorimeters because it offers excellent energy resolution and linearity at a reasonable cost.

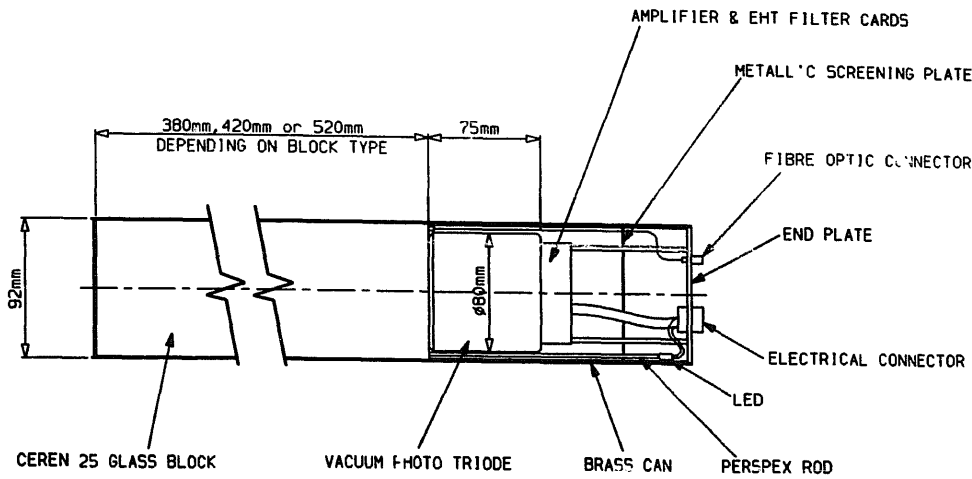


Fig. 4. A leadglass counter showing electrical and optical connections.

The energy resolution of leadglass calorimeters is generally considered [7] to be limited by three types of shower-by-shower fluctuations:

- intrinsic shower development;
- photoelectron yield;
- shower leakage.

Electronic noise may also degrade the resolution. The OPAL EMEC has been designed to maximise the signal to electronic noise ratio and minimise the effects of shower-by-shower variations on the energy resolution.

2.1. Assembly components

Fig. 4 is a schematic view of a leadglass assembly. The glass block is housed in a brass can of wall thickness 0.45 mm. This acts as an electrical screen and provides mechanical support for the assembly via the end plate of the can which is secured to a rigid back plate. This method of support permits an individual assembly to be withdrawn from the array without disturbing its neighbours. The surfaces of the leadglass blocks are polished. The block is wrapped (excluding the end to which the VPT is attached) with aluminium foil, which is at ground potential, and is enclosed in a protective layer of mylar.

2.1.1. Leadglass

The properties of the leadglass, CEREN 25 [8], are summarised in tables 1a and 1b. The external transmission coefficient of a 25 mm sample in air is shown in fig. 5 for a range of wavelengths. Note that an internal transmission of 1.0 gives an external transmission of 0.88 because of reflections at the air-glass interfaces. The spectrum of generated Cherenkov light is peaked towards short wavelengths, and thus it is important that the CEREN 25 transmission (table 1b) extends to wavelengths below 400 nm.

In order to locate the position of an electromagnetic shower precisely within the calorimeter, it is necessary for the energy to be shared between a number of leadglass blocks. Balancing this requirement against that of increasing cost for improved granularity, led to a choice of block cross-section of $92 \times 92 \text{ mm}^2$. (The wrapping, brass can and clearance between the counters add 2 mm, so the counters are mounted on a 94 mm pitch.)

The front faces of the EMEC calorimeters are arranged to follow the contours of the central detector pressure vessel. The outer circumference of the Dees is brought as close as possible to the coil of the solenoidal

Table 1a

Corning CEREN 25 properties [8] (Chemical composition by weight)

SiO ₂	- 39%
PbO	- 55%
K ₂ O	- 2%
Na ₂ O	- 3%
- Density:	4.06 g/cm ³
- Radiation length (X_0):	2.51 cm
- Refractive index:	1.708 (at 400 nm)
- Linear coefficient of thermal expansion (20-300 °C):	$74 \times 10^{-7} / ^\circ\text{C}$

Table 1b

Corning CEREN 25 properties [8] (Internal transmission for wavelength of 400 nm)

Thickness (X_0) (radiation lengths)	Transmission
10	0.981
25	0.954
50	0.910
100	0.829

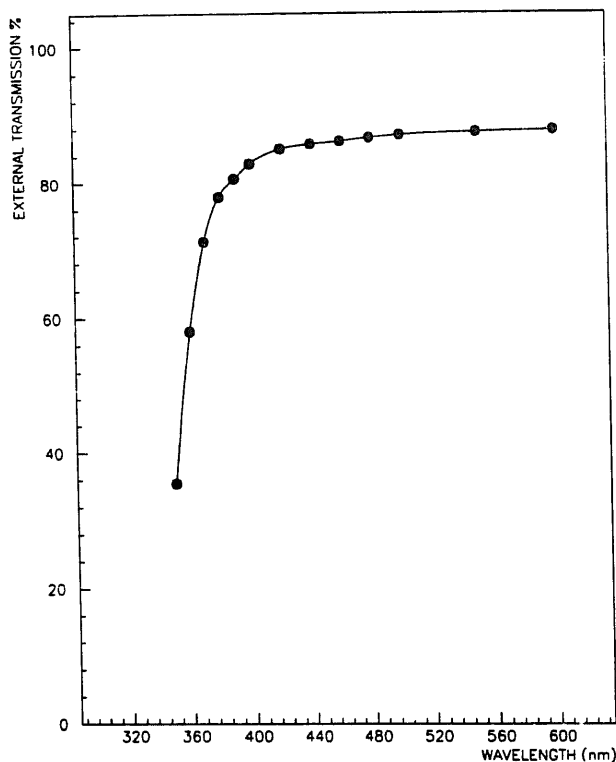


Fig. 5. The external transmission of a 25 mm sample of CEREN 25 in air as a function of wavelength. The line through the points is a spline fit drawn to guide the eye.

magnet to ensure complete overlap between the barrel and end cap calorimeters. In addition presampler chambers are mounted on the front of the assemblies. Within these tight geometrical constraints it was not possible to arrange the modules so that each one pointed towards the interaction region.

A consequence of the nonpointing geometry is that (away from the forward direction) particles enter the leadglass at oblique angles. The block lengths are chosen to give a total depth of at least 20.5 radiation lengths for all allowed trajectories within OPAL. This is discussed further in section 5.

2.1.2. Vacuum photo triodes

The vacuum photo triodes are optically coupled to the leadglass by an epoxy resin, selected for optical clarity and high refractive index. The ingredients were supplied by CIBA Geigy; the properties are summarised in table 2.

The VPTs are supplied by Philips [9]. Comparisons with triodes from other manufacturers have been made in previous papers [4]. Fig. 6 shows a schematic view of the triode. Photoelectrons, emitted from the photocathode are accelerated through a potential difference of 1200 V towards the grounded anode grid. Most are transmitted through the grid and continue until they hit the dynode which is at a potential of -600 V with

Table 2
Glue properties

Resin:	Di-glycidyl Ether – Bisphenol A
Hardener:	Aliphatic Amine – Tri-methyl hexa-methylene diamine
Refractive index = 1.63 ± 0.02 in the visible region	

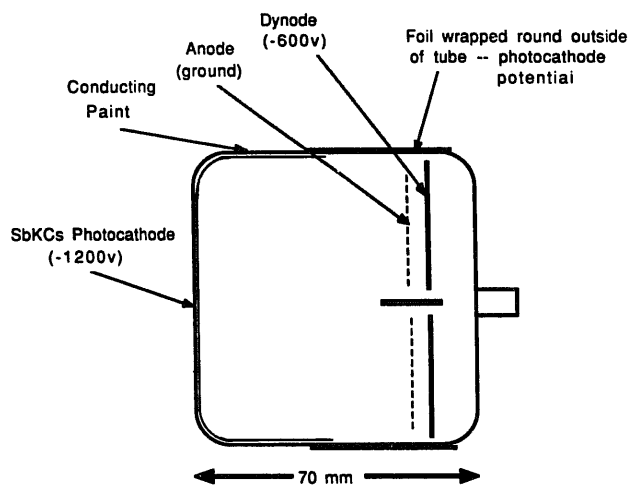


Fig. 6. Schematic cross-section through Vacuum Photo Triode.

respect to earth and is placed directly behind the anode. Electron multiplication then occurs, and the secondary electrons are attracted back to the anode. The properties of the Philips VPTs are summarised in table 3. The D-type photocathode is characterised by a low dark current and high quantum efficiency, which is peaked at wavelengths well matched to the spectrum of Cherenkov light transmitted by the leadglass.

Fig. 7 shows the distribution of triode gains measured in an axial magnetic field of 0.7 T. The mean of the distribution is 11.5. At 0.4 T, the mean is 13.5.

Fig. 8 shows the measured "Corning Blue" * sensitivities for the triodes. The mean of $10.8 \mu\text{A}/\text{lumen}$ corresponds to an average peak quantum efficiency of 26%. As discussed below, this excellent sensitivity contributes to the achievement of good energy resolution.

* The quantum efficiency of a photosensitive device is defined as the ratio of the number of emitted photoelectrons to the number of incident photons. Since the efficiency is strongly wavelength dependent, it is normally measured with the use of an accurately specified illumination. The standard light source employed for testing devices which are used to measure scintillation and Cherenkov light has light from a tungsten lamp at a temperature of 2856 K passing through a Corning CS No. 5-58 filter. This generates a spectrum centred at ~ 420 nm. Corning Blue (CB) sensitivity is then defined as the cathode sensitivity measured in $\mu\text{A}/\text{lm}$ (after the filter) using the above defined light source.

Table 3
Vacuum photo triode properties

Type:	RTC 1501/FL
Nominal photocathode diameter:	3 in.
Photocathode:	D type-Sb K Cs
Average gain (at 0.4 T):	13.5
Average quantum efficiency ^{a)} (with CB source):	26%
Overall diameter:	80 mm
Length (excluding vacuum seal):	70 mm
Maximum operating voltage:	1200 V

^{a)} At peak sensitivity in the spectral response.

2.1.3. Electronic chain

The high voltage and signal readout circuitry used with the triodes is shown in fig. 9. The need for significant post amplification makes careful ripple filtering of the high voltage supply very important. This is achieved with a two-stage low-pass filter which gives attenuation of around 50 dB at 50 Hz and 154 dB at 20 kHz. A voltage supply with 1 V rms of ripple at 20 kHz produces only 33 nV rms of ripple at the VPT. This would result in a noise signal at the amplifier output equivalent to 2 or 3 electrons rms.

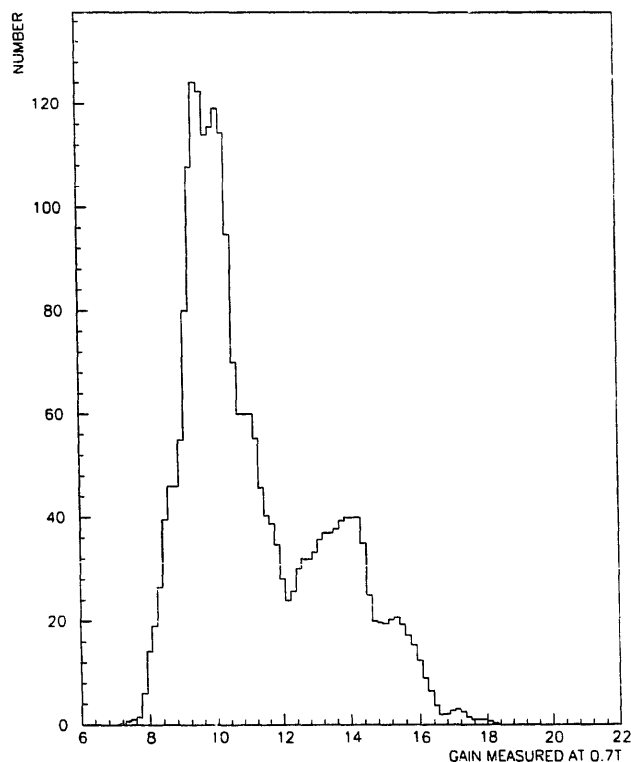


Fig. 7. The distribution of triode gains measured at a magnetic field of $B = 0.7$ T for the full triode sample. The gain increased through the production cycle and the curve shows a superposition of several distributions.

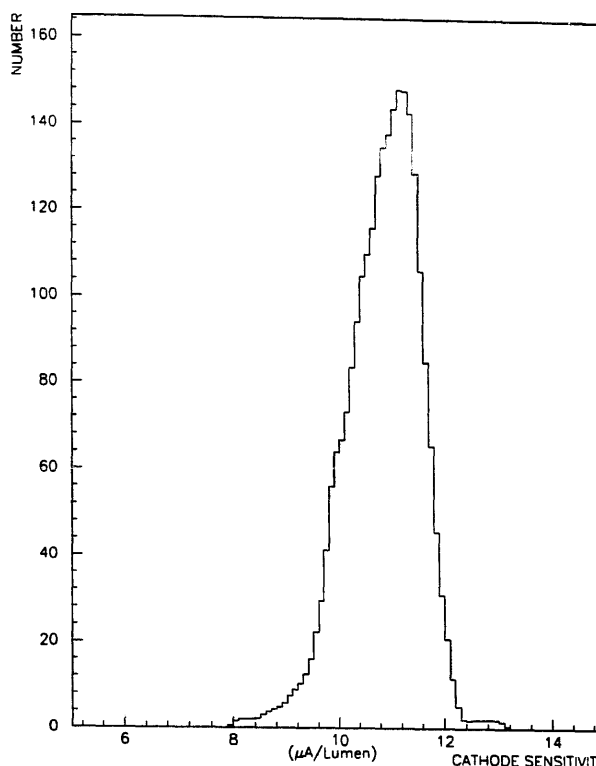


Fig. 8. The distribution of Corning Blue measurements for the full triode sample (see text for definition of "Corning Blue"). Note the good uniformity throughout the production. The peak quantum efficiency is approximately ($2.4 \times$ Corning Blue measurement) %.

The internal gain factor of a VPT is only of order 10–20. It is therefore necessary to amplify the output signal with a high-gain, low-noise amplifier before it can be accepted by an ADC. An amplifier has been specially developed for this application at the Rutherford Appleton Laboratory [10].

At LEP the interval between beam crossings is 22 μ s. This makes it possible to improve the noise performance of the amplifier by shaping the signal with relatively long time constant. Fig. 10 shows the signal waveform measured at the input of the ADC. The amplitude approaches zero to within 1% of the peak value 22 μ s after the start.

The signal from the amplifier is transmitted to the electronics hut through a screened twisted pair cable to prevent noise "pickup". A pulse transformer provides matching between this cable and the 50 Ω coaxial cable feeding the input of the Analogue to Digital Converter (ADC) [11]. Although the ADC input impedance is 50 Ω , it requires a source impedance of greater than 150 Ω for satisfactory noise performance. This requirement is met by a resistive attenuation network which also allows the overall response of each channel to be adjusted over a range of 4:1 providing the channel to channel matching needed for physics-event triggering purposes.

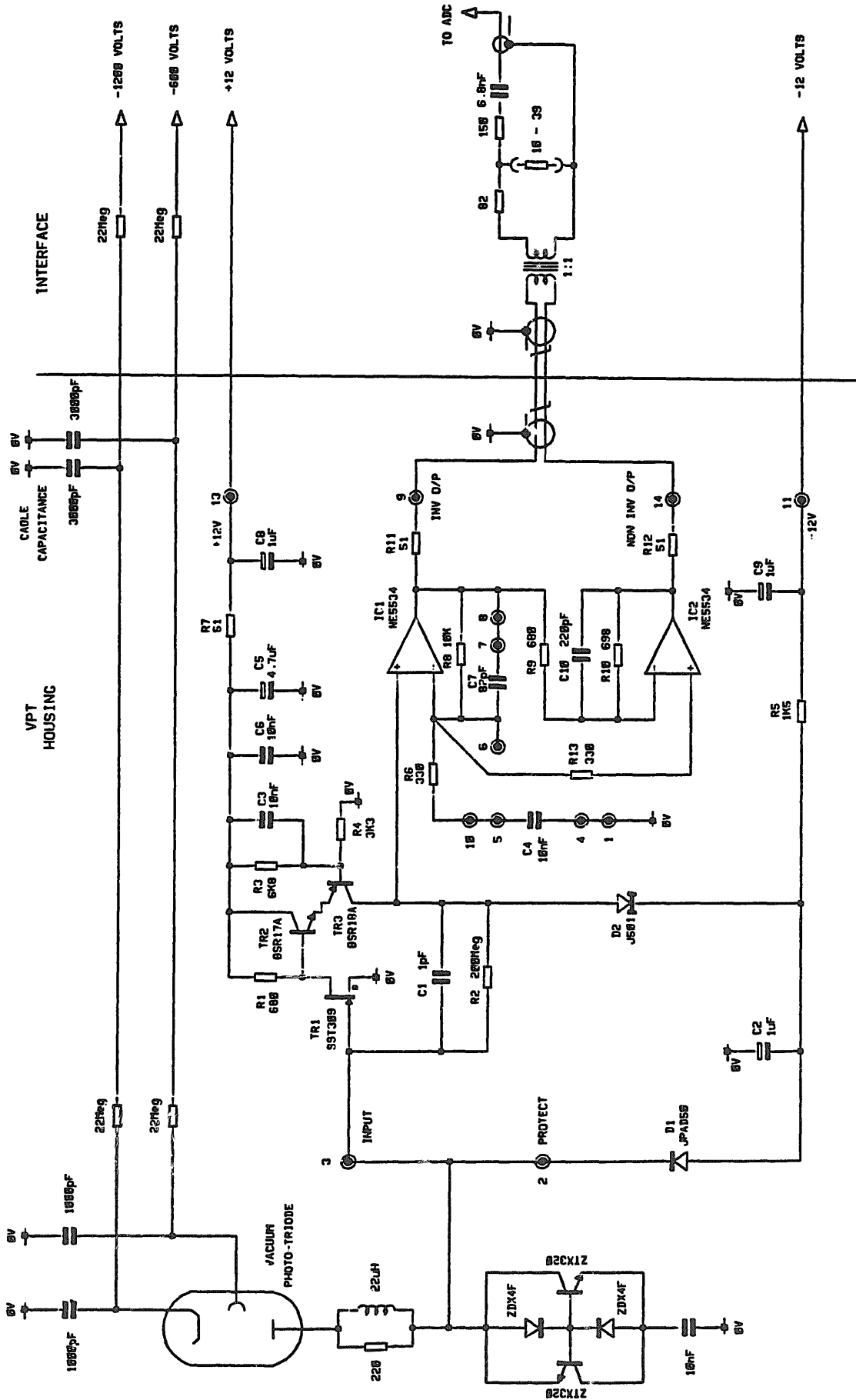


Fig. 9. Circuit diagram of complete triode detector including preamplifier and associated components.

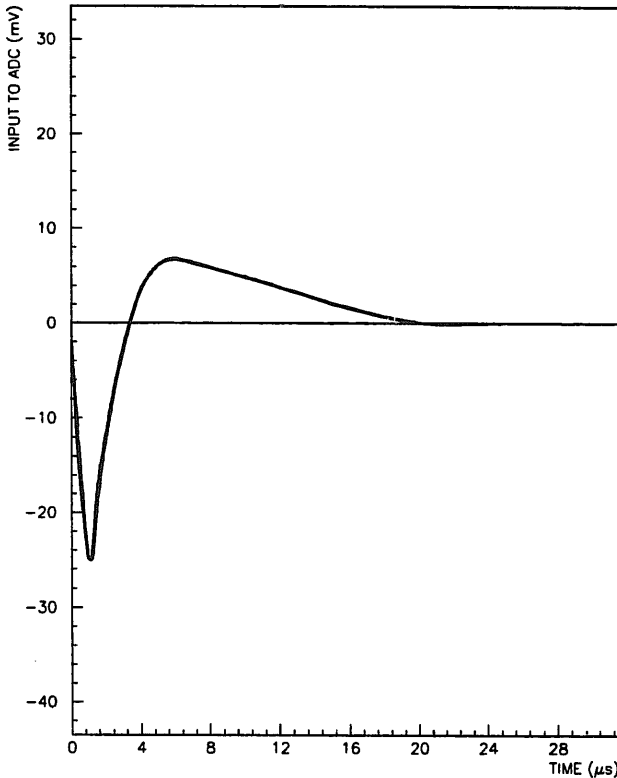


Fig. 10. Signal waveform at ADC input.

2.1.4. Light sources

Each assembly has two reference light sources (fig. 4) which are used for monitoring its performance. In one system light is taken via optical fibres to each counter from a liquid scintillator cell which is excited by a pulsed ultraviolet nitrogen laser. A fibre optic connector joins the external fibre to an internal fibre which injects light into the corner of the leadglass block. A full description of this system is given in OPAL 2. The scintillator has been chosen to give a spectrum of light which is similar to the spectrum of Cherenkov light transmitted by the leadglass blocks.

Each assembly also has a green light emitting diode (LED). The LED is mounted on a perspex rod which is glued to the end of the leadglass block (fig. 4). This arrangement obviates electrical signals passing near the very sensitive amplifier. The green LEDs generate light over a broad spectrum with an average wavelength of 565 nm. With the laser-driven system all channels must be pulsed together. The LED system allows an individual channel or any subset of channels to be selected (OPAL 2).

2.1.5. Photoelectron yield and noise considerations

The mean number of photoelectrons produced by an electromagnetic particle with incident energy E (in units of GeV) is found to be $1.8E \times 10^3$ (see section 4.7).

Thus the contribution to the overall energy resolution from photoelectron fluctuations (at $B = 0.4$ T) is:

$$\left(\frac{\sigma_E}{E}\right)_{\text{p.e.}} = \left(\frac{1 + g^{-1}}{1800E}\right)^{1/2} = 0.027/\sqrt{E},$$

where g is the gain of the triode (at $B = 0.4$ T), and E is the energy of the shower in GeV. Note that the second term represents fluctuations at the dynode.

The noise level at the output of the amplifier corresponds to 175 electrons rms at the input, with the input open circuit. This is increased by an additional 4 to 5 electrons rms per pF of shunt capacitance across the input. Since the VPTs have a capacitance of ~ 30 pF between anode and earth, the electronic noise referred to the amplifier input with VPT connected is ~ 300 electrons rms.

If we assume that it is necessary to sum over n channels to collect all the energy from an electromagnetic shower, then since the amplifier noise is stochastic the contribution to the overall energy resolution is:

$$\sqrt{n} \frac{300}{1800Eg} \times 100\%.$$

The coherent noise across an array of assemblies is measured to be negligible.

It is interesting to consider the performance which would have been obtained if vacuum photo diodes had been used. These have been used successfully with scintillator detectors in other experiments [12], however, the light output per unit energy deposited by an electromagnetic shower is two to three orders of magnitude less from leadglass than from sodium iodide for example. The shunt capacitance of a photo diode is less than a triode, but neglecting this difference, we estimate that a 1 GeV electromagnetic shower shared between 2 leadglass blocks instrumented with photo diodes would suffer an electronic noise contribution of about 25% to the energy resolution. Triodes, with an average intrinsic gain of 13.5 (at $B = 0.4$ T) reduce this to less than 2%.

The discussion of the contributions which, when combined, determine the energy resolution is continued in section 5.

3. Studies in electron beams at CERN

In order to establish the anticipated performance of the EMEC experimentally it is necessary to carry out measurements over a wide range of energies under conditions which are close to those foreseen in OPAL. It is crucial to do at least some of the studies in an axial magnetic field, because shower development and VPT behaviour may differ significantly from the zero field case.

Two experimental arrangements are reported. One measures the performance of single counters when sub-

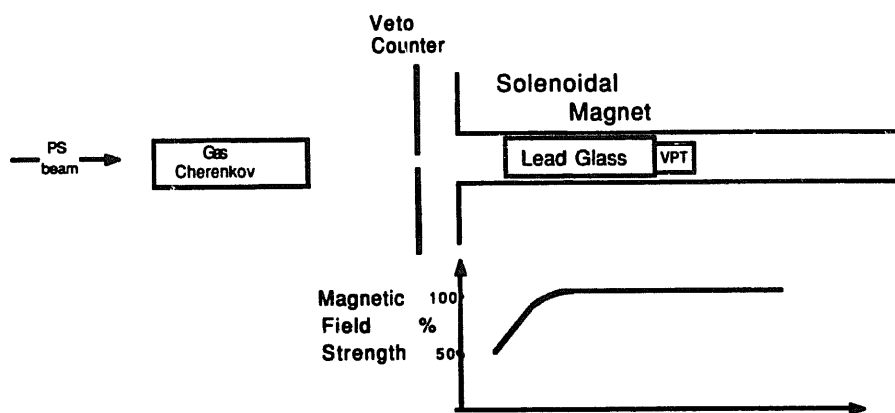


Fig. 11. Schematic view of experimental setup for beam tests at the CERN Proton Synchrotron.

jected to the axial magnetic field of a solenoid. This is described in section 4. The second measures the response of an array of assemblies operating in the absence of an applied magnetic field and is reported in section 5. Many of the experimental details for the two arrangements, however, are common and are given below.

Figs. 11 and 18 show the beam-line arrangements. The portion of beam striking the centre of the leadglass block is selected with scintillation counters. Electrons are identified using the threshold gas Cherenkov counters. In order to prevent charge "pileup" in the amplifier, events are rejected if a second particle arrives in the time interval from 20 μs before to 5 μs after the particle initiating the trigger. Such precautions are not needed in operations at LEP because of the 22 μs interval between bunch crossings.

The output from the amplifier is measured with a charge sensing ADC operating with a gate length of 2 μs (set symmetrically about the negative portion of the bi-polar pulse). The long ADC gate effectively reduces the overall bandwidth, and noise levels are reduced by $\sim 15\%$ compared to the value obtained using a peak sensing ADC. The gate length is chosen to maximise the signal-to-noise ratio.

The mean pulse height for electrons of given energy is determined from a Gaussian fit to the measured pulse height distribution. In the results presented in sections 4 and 5, the distributions are truncated within the limits of ± 3 standard deviations from the mean.

4. Detector characteristics in an axial magnetic field

This section describes the response of a single assembly to electromagnetic particles whilst subject to an axial magnetic field. The experiments are conducted in the T10 beam at the CERN PS, and the experimental arrangement is shown in fig. 11. Each assembly in turn

is positioned in the solenoidal magnet [13] so that the VPT is in the uniform central part of the axial field.

The spread in momenta of particles transported by the T10 beam (approximately 2% rms) makes a significant contribution to the width of the energy distribution measured in the leadglass.

An estimate of the beam momentum spread has been made by finding the value, assumed to be independent of momentum which, when unfolded from the measured

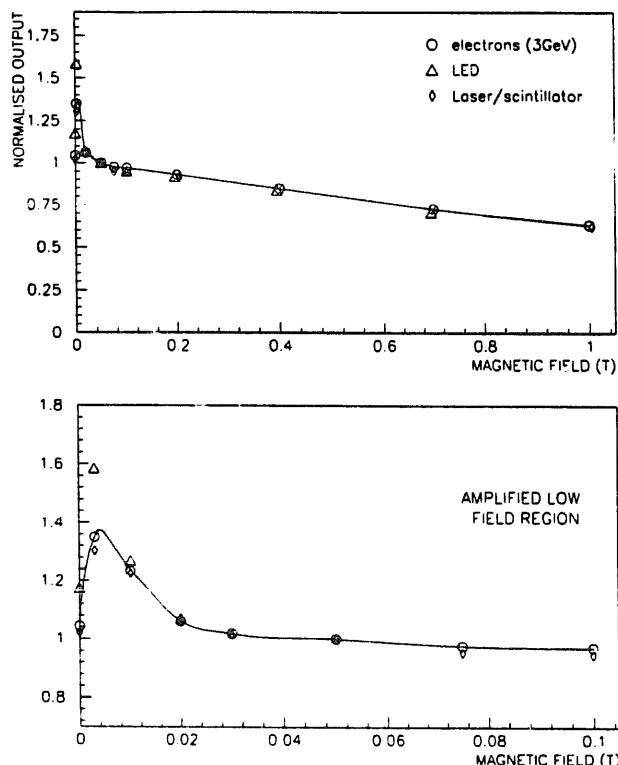


Fig. 12. Triode output as a function of applied axial magnetic field for three different sources of light, measurements normalised to reading at $B = 0.05$ T. The lines through the electron points are spline fits drawn to guide the eye.

energy distributions at different energies, leads to the expected $1/\sqrt{E}$ dependence for the intrinsic resolution. The $1/\sqrt{E}$ dependence is confirmed by other measurements on these counters made at the CERN SPS and with similar devices at DESY. By using particles with momenta in the range $0.5 \rightarrow 3.0$ GeV/c, a rms momentum bite of 1.7% is derived for the collimator settings used in these tests. All subsequent data from the T10 test beam have this component unfolded from the energy resolution.

4.1. The response as a function of magnetic field

Fig. 12 shows typical VPT output as a function of axial magnetic field for electrons, LED and scintillator/LASER light sources (each curve is normalised to the measurement at 0.05 T). At higher fields all three light sources show excellent agreement; below 0.02 T the scintillator source follows more closely the behaviour of the electrons than does the LED source.

A detailed attempt to understand the low-field behaviour has not been made, but the following qualitative description gives a plausible explanation of the features. At very low magnetic fields, the sharp rise in gain with increasing magnetic field is related to the details of the VPT geometry. There is a loss in gain at very small magnetic fields because photoelectrons follow the electric field lines to the small rod which passes through the hole in the centre of the anode (fig. 6) thereby missing the dynode. This loss falls rapidly with increasing magnetic field as the photoelectrons begin to follow more closely the magnetic field lines. The photocathode surface area is larger than the anode or dynode. At very low magnetic fields photoelectrons emitted from the perimeter of the photocathode are focused towards the anode by the electric field. At higher magnetic fields they pass outside the anode area resulting in reduced output. The differing response for LED and scintillator/LASER light sources at low fields may reflect the different way the photocathode response varies as a function of wavelength across the surface, or the different helical paths followed by the photoelectrons resulting from their different emission energies. For applied magnetic fields greater than 0.05 T, the above effects saturate and the output slowly decreases with field as a result of the anode grid transmission (through to the dynode) gradually reducing. At 0.1 T the gain is typically 15 for an applied voltage of 1200 V and it falls approximately linearly with field reaching a value of around 10 at 1 T.

4.2. The VPT gain

The gain of a VPT is measured by operating the detector under identical conditions first as a triode, then as a diode, and taking the ratio of outputs. Fig. 13

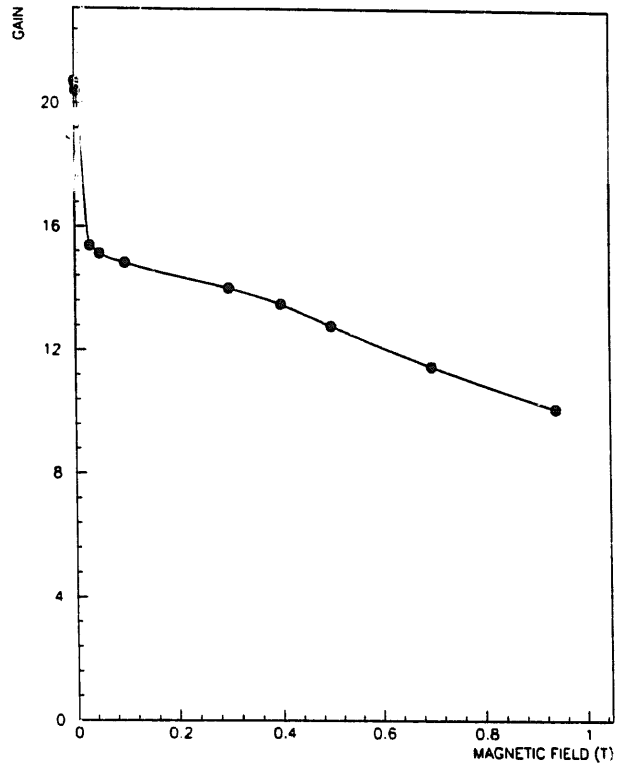


Fig. 13. Triode gain as a function of applied axial magnetic field averaged over complete triode sample (1200 V applied). The line through the points is a spline fit drawn to guide the eye.

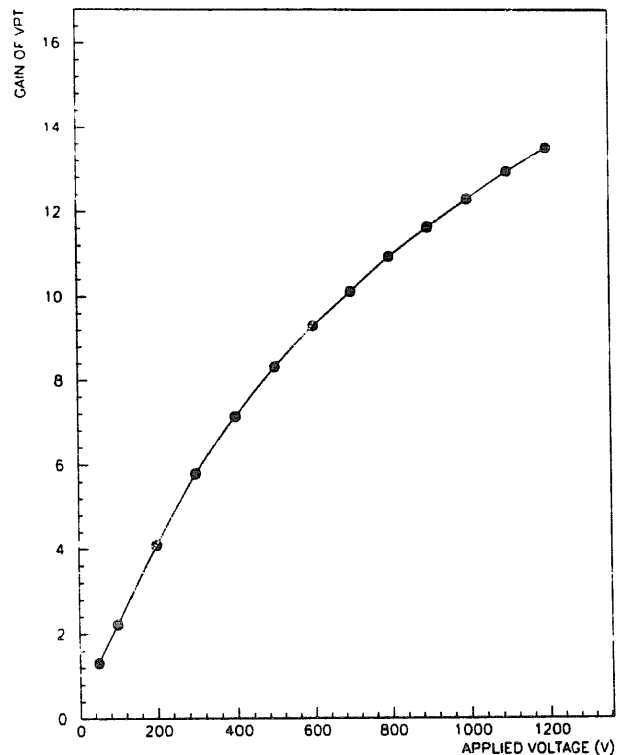


Fig. 14. Triode gain as a function of applied voltage at $B = 0.4$ T. The line through the points is a spline fit drawn to guide the eye.

shows the gain averaged over our entire triode sample measured as a function of axial magnetic field. Note that at 0.4 T (the initial operational field for OPAL) the average gain is 13.5 at an applied voltage of 1200 V.

Fig. 14 shows the gain as a function of applied voltage for an applied magnetic field of $B = 0.4$ T. It can be seen that the triode output is insensitive to small changes of high voltage, a change of 10 V leading only to a change in gain of 0.5% at 1200 V.

4.3. The "equivalent noise" of a detector

The electronic noise is discussed in section 2.1.5. The overall noise (which also includes pickup and ADC noise) can be expressed in units of energy as the "equivalent noise" of a detector. In units of MeV, it is defined as σ/m where:

σ = rms width of the "pedestal" distribution (the ADC output with no signal present)
 m = mean (pedestal subtracted) ADC signal for an electromagnetic shower of energy 1 MeV which is fully contained within the calorimeter.

The average equivalent noise measured over the full triode sample is 10.7 MeV for an applied axial magnetic field of 0.03 T. The numerator of this ratio is almost independent of magnetic field, but since the denominator is a function of axial field (see fig. 12), then the equivalent noise must vary accordingly. Even at the full axial field of 0.4 T, the equivalent noise remains less than 13 MeV for a single assembly.

4.4. Measurement of energy resolution for a single detector

The transverse dimensions of a single detector are insufficient for it to contain all the energy from a high-energy electromagnetic shower. Thus the resolution obtained here has a natural lower limit due to leakage fluctuations; results with full lateral containment are presented in section 5.1. In these measurements a block of length $20.5X_0$ is used, enough to provide full longitudinal containment at PS energies (up to 5 GeV).

The single block energy resolution for 3 GeV electrons, plotted as a function of axial magnetic field, is shown in fig. 15.

Fig. 16 shows the energy resolution plotted as a function of energy. The normalised energy resolution is better than $5\%/\sqrt{E}$ at all energies up to 5 GeV.

4.5. Effects of non-axial magnetic field

The vacuum photo triodes have been developed specifically for applications where the direction of the magnetic field is close to the axis of the triode [14]. However, such VPTs, have acceptable gain even when the magnetic field makes a significant angle with the axis, as shown in fig. 17, where the relative output is

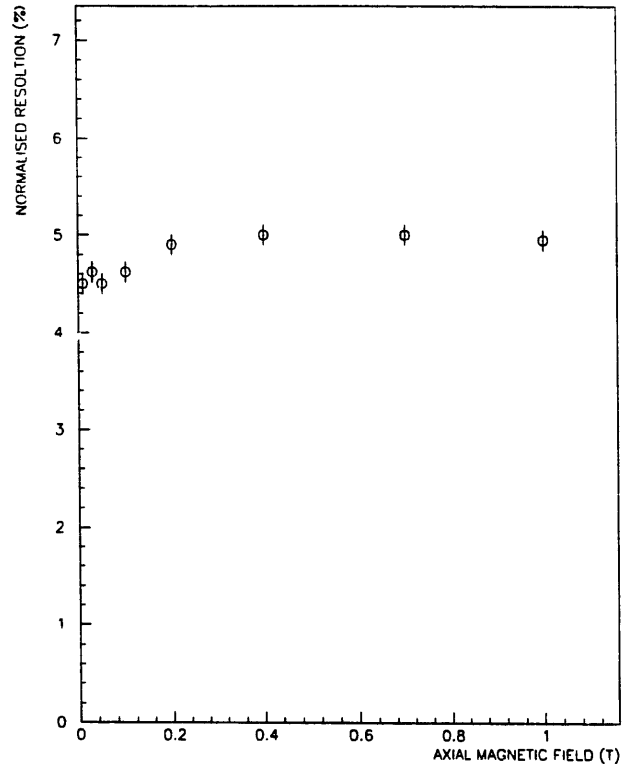


Fig. 15. Normalised energy resolution as a function of applied axial magnetic field for a single block measured with electrons of energy 3 GeV.

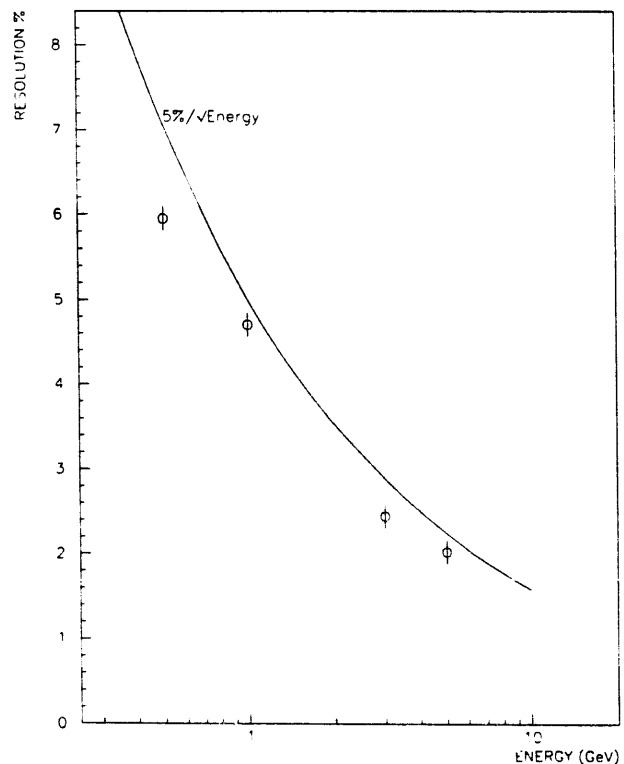


Fig. 16. Energy resolution as a function of energy (measured at the CERN Proton Synchrotron) for a single assembly subjected to a magnetic field of $B = 0.4$ T.

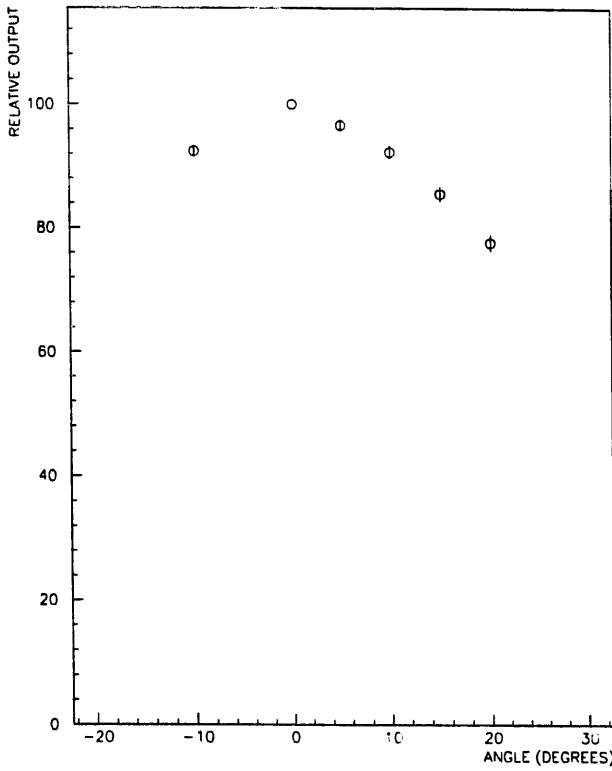


Fig. 17. Triode output as a function of angle of magnetic field with respect to triode axis in a field of 0.03 T. A blue LED light source was used for these measurements.

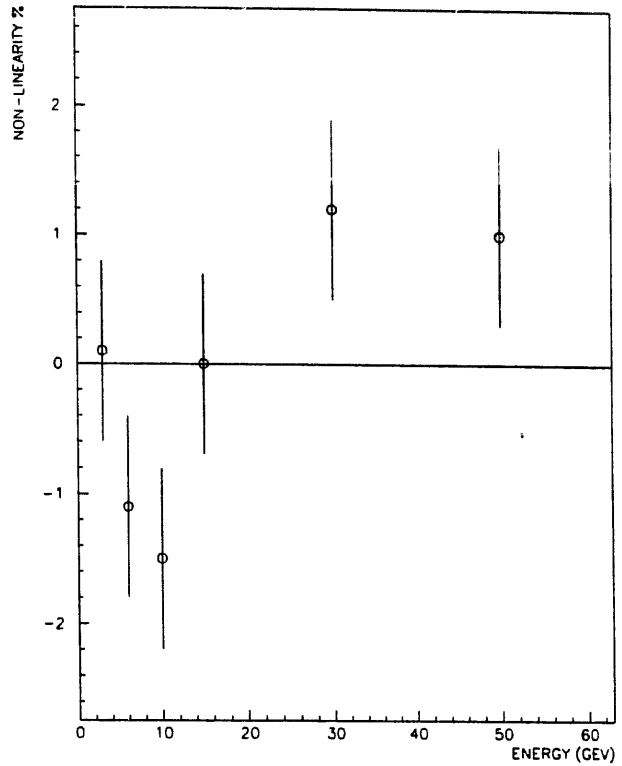


Fig. 19. Percentage nonlinearity defined as the percentage deviation from a linear relationship as a function of energy.

plotted as a function of this angle. The measurements were made with a blue LED light source illuminating the photocathode uniformly and with an applied magnetic field of 0.03 T. The angular dependence does not change significantly at higher magnetic fields.

4.6. "Reversed" detectors

In order to have complete overlap between the end cap leadglass detector and the forward detectors of

OPAL, the inner rings of leadglass (closest to the beam pipe), are mounted with the triode end closest to the interaction point. Thus particles pass through the triode before reaching the glass. Assemblies have been tested in the solenoid with this "reversed" orientation and compared with the usual arrangement where particles enter an assembly directly through the glass. For these measurements an axial magnetic field of 0.4 T is used and a beam of 3 GeV electrons. A relative decrease in output of 16% is found with a normalised energy resolution of $(\sigma_E/E)\sqrt{E} = 4.7\%$.

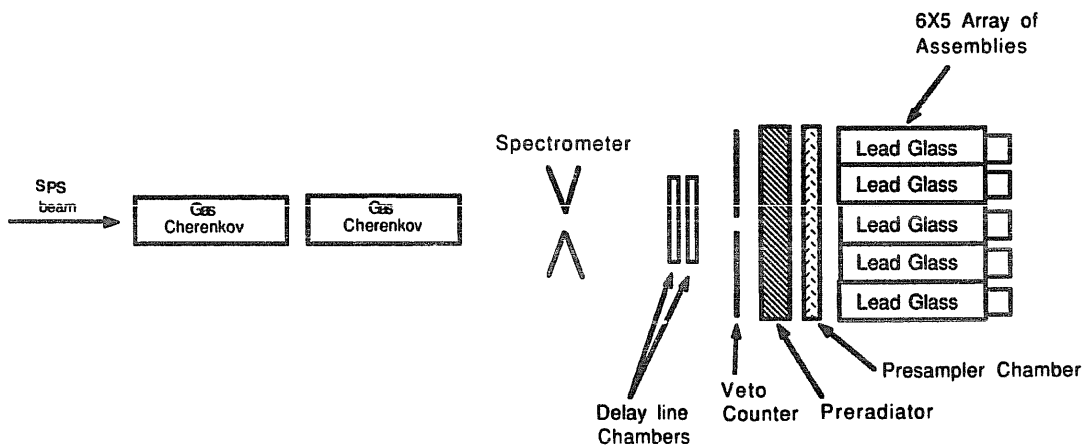


Fig. 18. Schematic view of experimental setup for SPS beam tests.

4.7. Relating photoelectron yield to shower energy

As already mentioned, in a field of 0.4 T the photoelectron yield, (the average number of photoelectrons produced by an electromagnetic particle with energy E (GeV) is $1800E$. This is established from the width of the pulse height distribution obtained with the LED source adjusted to give the same signal amplitude as a fully contained 1 GeV shower. (Electromagnetic showers cannot be used directly for this estimation because of the inherent fluctuations in light yield.) Fluctuations in the number of incident photons and in the yield of secondary electrons at the dynode are taken into account in the calculation.

5. Detector characteristics determined with an array of leadglass assemblies

This section describes the response of an array of leadglass assemblies in the X5 beam at the CERN SPS. The leadglass array can be moved vertically, horizontally and rotated about a vertical axis. The arrangement is shown schematically in fig. 18. There is no applied magnetic field. Since the momentum bite of the X5 beam is 7%, a magnetic spectrometer instrumented with

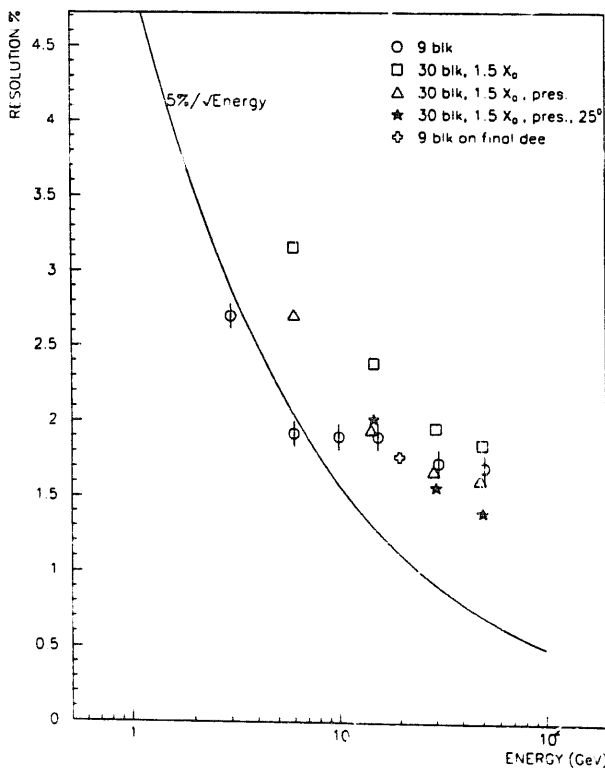


Fig. 20. Energy resolution as a function of energy for an array of counters at zero magnetic field, under different conditions.

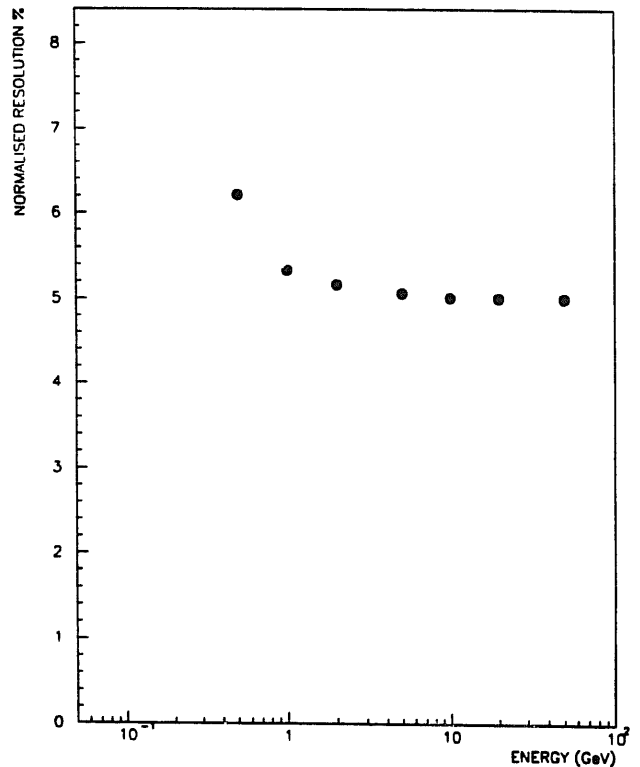


Fig. 21. Predicted normalised energy resolution as a function of energy. A normalised energy resolution of $5\%/\sqrt{E}$ is assumed and the effect of electronic noise is included. For energies up to 1 GeV energy is assumed to be summed over 2 blocks, up to 4 GeV over 4 blocks, up to 15 GeV over 9 blocks and for higher energies over 25 blocks.

multiwire proportional chambers (MWPCs) is employed to calculate the momentum of each beam particle.

The beam energy can be set in the range between 3 and 50 GeV, and the beam intensity is typically 1000 particles in a spill time of 2.8 s.

The beam spectrometer momentum resolution is dominated by multiple scattering at low energies, and by MWPC position resolution at high energies (0.48% rms at 6 GeV, 0.25% rms at 50 GeV). These contributions to the measured leadglass energy resolution have been unfolded from the results presented below.

The beam is aligned centrally into each counter in turn to calibrate it before further measurements are made. An energy of 20 GeV has been used for this exercise.

5.1. The linearity of detector response

The energy linearity is measured in the range 3 to 50 GeV for a 9 block array of detectors with block length $20.5X_0$ along the beam direction. Fig. 19 shows the relation between the nonlinearity (where this is defined as the percentage deviation (measured-predicted) from a completely linear relationship) and the beam energy.

It is known that at higher energies the shower penetrates beyond the end of the leadglass block. The excellent linearity observed is attributed to the following compensating mechanism. The Cherenkov light from showers which develop deep in the block suffers less attenuation before it reaches the VPT, and this compensates for the loss of shower energy from the back of the block.

5.2. The energy resolution of an array of detectors

At energies of a few GeV or less most of the energy of an electromagnetic shower can be contained laterally in a single block and it can be measured with good resolution. At higher energies, fluctuations in the lateral energy loss become important and it is necessary to use an array of counters to investigate in a test beam the performance to be expected in OPAL.

There is a further complication since the fluctuations in the energy loss from the back of the counters limits the resolution above energies of about 10 GeV. In OPAL there is a considerable amount of material in the front of the counters (the end plates and pressure vessel of the central tracking chamber) and this reduces the leakage from the back of the counters. In addition particles enter at non-normal incidence. The presampler chambers positioned in front of the leadglass (see fig. 2) give an estimate of the energy deposited (on a shower-by-shower basis) in the passive material, reducing the loss in energy resolution due to fluctuations in shower development here. The presampler measurements given in this paper use prototype equipment which was not optimised. They are presented simply to give an idea of what can be achieved. More detailed results will be given in a forthcoming paper [15].

The energy resolutions presented in this section have electronic noise contributions subtracted. The effects of noise are considered in section 5.3.

Fig. 20 presents the energy resolution plotted as a function of energy (on a logarithmic scale) under a number of different arrangements. The energy dependence of the energy resolution for a nine block array with no material in front is well described by the expression $\sim 5\%\sqrt{E}$ below 6 GeV, but becomes relatively worse at higher energies. There is good agreement with the single block results shown in section 4.4.

Adding 1.5 radiation lengths of lead in front of the leadglass reduces shower leakage from the back. In addition the electromagnetic shower starts earlier and is therefore more spread laterally. The energy deposited in the glass is in general lower because of the energy lost in the lead, and the resolution is degraded because of fluctuations in this quantity. Results are shown in fig. 20 for a 30 block array with a $1.5X_0$ radiator in front. At 50 GeV the improved containment almost exactly

compensates for the increased fluctuations in energy caused by the lead.

The energy lost in the material in front of the glass can be compensated on a particle-by-particle basis using a presampler. Fig. 20 also shows results obtained with a prototype of the thin gap high gain chamber to be used in OPAL. The resolution is considerably improved. At 15 GeV the resolution is recovered to the value with no passive material, and at 50 GeV the overall energy resolution is improved.

In the analysis presented here, the presampler correction is made in the following way. The total energy (E) deposited by an electromagnetic shower is:

$$E = L + \lambda(E)P,$$

where L is the energy measured in the leadglass; P is the pulse height recorded in the presampler chambers. The constant $\lambda(E)$ is chosen to optimise the resolution of the total energy (E) for a given energy.

Finally, fig. 20 shows results obtained with a 30 block array and a radiator and presampler, with particles entering the leadglass at an angle of 25° with respect to normal incidence. At the highest energies the energy resolution is improved compared to the normal incidence case because of the greater projected depth of glass which reduces energy leakage.

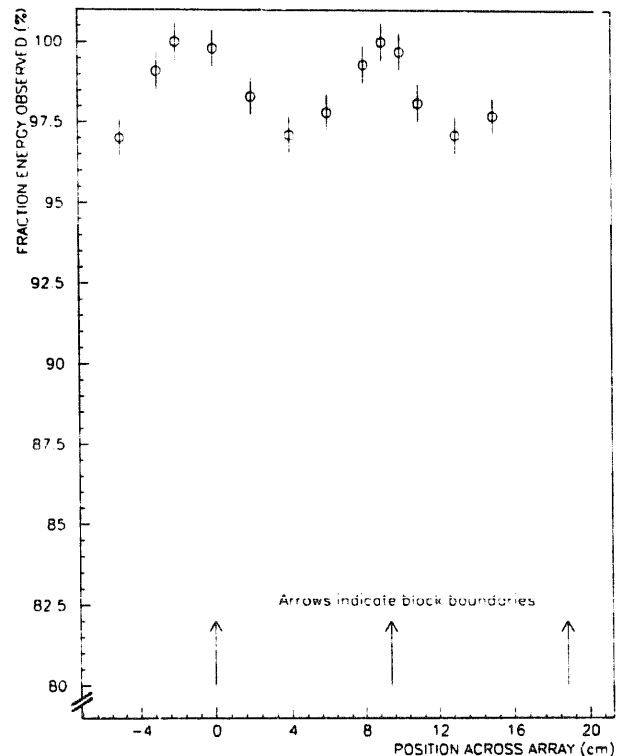


Fig. 22. Fraction of incident energy observed at different positions across leadglass array, measured with a 15 GeV electron beam with an angle of incidence of 15° with respect to normal. (Zero magnetic field.)

5.3. The effect of electronic noise contributions to energy resolution

The equivalent noise for an assembly operating in a magnetic field of 0.4 T is ~ 13 MeV. In general it is necessary to sum the signals from several blocks to obtain the total energy deposited by a single electromagnetic shower. If the noise is stochastic the total noise is obtained by adding the separate contributions in quadrature. Measurements on a complete Dee confirm that any contributions from correlated noise, which would add coherently, are indeed small. Fig. 21 shows the expected average effect of noise as a function of energy assuming that the energy resolution without contributions from noise follows the form $5\%/\sqrt{E}$. Note that the number of blocks used to sum the total signal deposited is also a function of energy. At 1 GeV the resolution is 5.3% and at 0.5 GeV it is 6.2%.

5.4. The variation in detector output as a function of position across the array

As well as good linearity, it is important that the calorimeter offers uniform response as a function of particle entry position. Fig. 22 shows the summed output as a function of position, obtained by scanning a 15 GeV beam of electrons (with beam spot diameter 25 mm) across three blocks. The beam is at 15° from normal incidence (a typical trajectory in OPAL). A variation of about 2% peak-to-peak is obtained. In OPAL, most blocks are staggered longitudinally with respect to their neighbours [16]. In addition the passive material in front of the leadglass will tend to spread the shower before it reaches the EMEC. For those reasons, and because the measurements were made at zero magnetic field, fig. 22 is not representative of OPAL.

5.5. The spatial resolution of the detector

Since electromagnetic showers spread across more than one assembly, and the energy is shared by neighbouring counters, this information can be used to determine the position of the incoming particle. The method used here is to calculate the ratio of pulse-heights in the neighbouring blocks. Position resolutions have been measured with 6 GeV electrons incident at 15° on a prototype 3×3 leadglass array, with no applied magnetic field. The spatial resolution varies in the range 8.3 mm to 13.8 mm rms, typical distributions are shown in figs. 23a, b and c. The spatial resolution is much improved at higher energies. In separate measurements made with the final detector, electrons fired centrally into a leadglass block at normal incidence gave position resolutions as shown in table 4.

In OPAL the position measurement derived from the leadglass will be complemented by data from the pre-

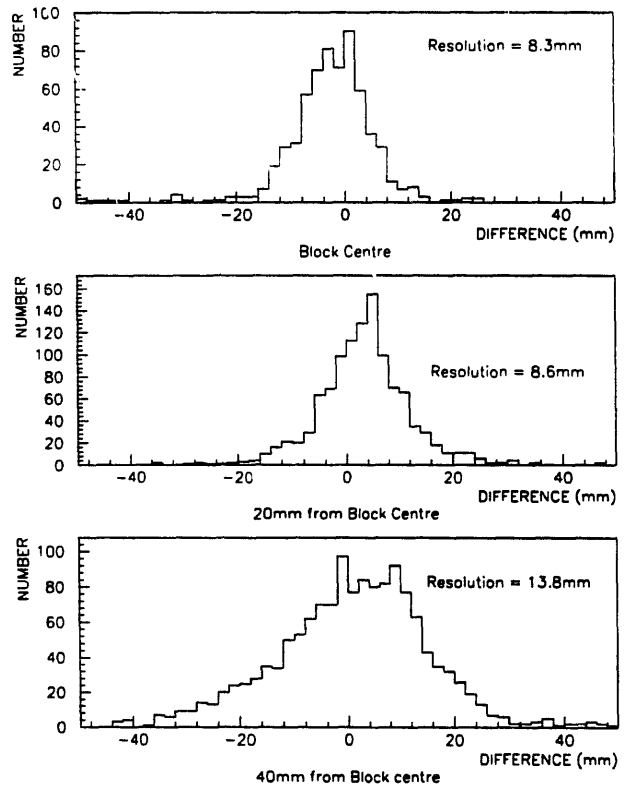


Fig. 23. Position resolution at three positions across the leadglass array for a 6 GeV electron beam incident at 15° to normal. (Zero magnetic field.)

sampler chambers, and for charged particles, from the central drift chamber.

5.6. Detector response to charged hadrons

The Cherenkov counters in the X5 beam can be used to veto electrons and thereby select a sample of hadrons. In general, showers initiated by hadrons contain both hadronic and electromagnetic particles. The two components propagate and deposit their energy quite differently in leadglass. Since the glass blocks are only of the order of 1 absorption length deep much of the hadronic energy leaks from the back of the counters. As a conse-

Table 4
Position resolution as a function of energy

Energy [GeV]	Position resolution ^{a)} [mm]
5	9.9
10	6.3
20	4.4
35	3.1
50	2.5

^{a)} Multiple scattering contributions which introduce an uncertainty in the predicted impact position and which amount to ~ 25 mm/E have not been unfolded from these numbers.

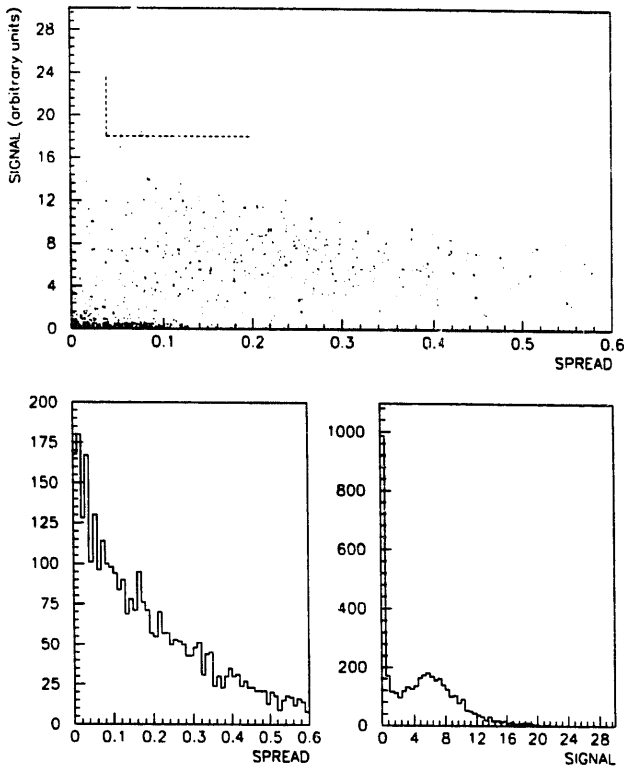


Fig. 24. Signal measured for 40 GeV hadron beam versus spread, where spread is defined as the ratio of energy summed in the 8 surrounding counters to the energy in the central counter.

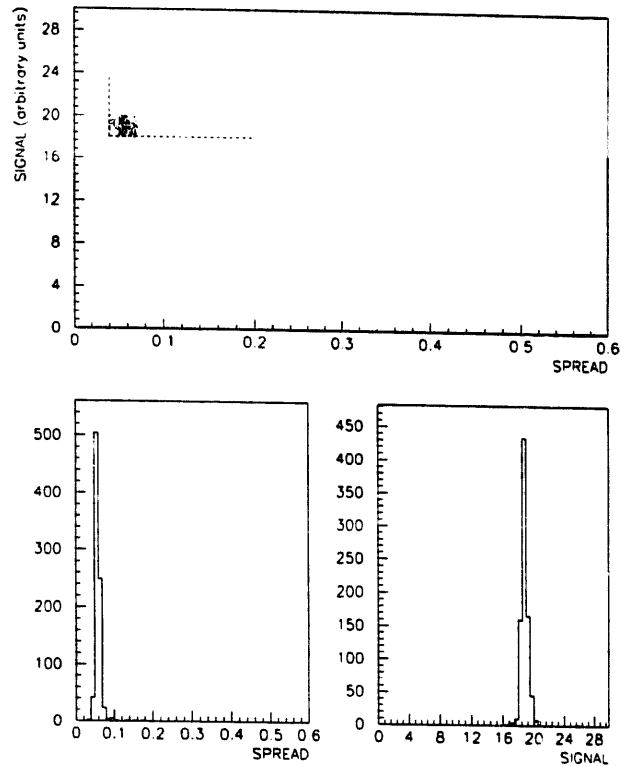


Fig. 25. Signal measured for 40 GeV electron beam versus spread, where spread is defined as the ratio of energy summed in the 8 surrounding counters to the energy in the central counter.

quence the variation in energy deposited by fixed energy hadrons can be very wide. Fig. 24 shows the energy recorded in the leadglass versus the lateral spread * for a sample of 40 GeV negative hadrons (pions). For comparison, fig. 25 shows an equivalent plot for electrons.

Particle identification is clearly possible using this information. In general, hadronic showers deposit less energy and are more widely spread than electromagnetic showers. Note that a small percentage of hadronic showers have an even smaller spread than electrons, and these form two categories. The first comprises noninteracting hadrons which give a small signal in the lead glass and the second, hadrons which travel most of the way through the glass but interact just in front of the triode.

The beam Cherenkov counters used to separate pions from electrons were not completely efficient and in fig. 24 there is a small electron contamination (of order 10 electrons). This background can be calculated on a statistical basis if the efficiencies of the Cherenkov counters are known.

* "spread" is here defined as the ratio of the energy summed in the 8 surrounding counters to the energy in the central counter.

The dotted lines on figs. 24 and 25 show cuts that could be applied to distinguish between hadronic and electromagnetic showers. For example with an electron detection efficiency of 90%, a hadron misidentification of 1 in 300 is obtained. The hadron rejection is defined as being the reciprocal of the misidentification.

At lower energies the separation is less clear and the hadron rejection reduces as shown in table 5.

6. Radiation damage and recovery of CEREN 25 lead-glass

Leadglass is susceptible to damage by ionising radiation which creates colour centres [17] causing strong absorption of light in the near ultraviolet, visible and near infrared.

Table 5
Hadron rejection for 90% efficiency

Energy [GeV]	Rejection
10	66 ± 11
20	134 ± 30
40	298^{+235}_{-91}

Two sets of measurements have been made to investigate the effect of radiation on CEREN 25 glass. In each case samples are arranged centrally between 4 radioactive sources consisting of rods of cobalt-60. The dose rate is 80 Gy/h and the radiation is uniform to within $\pm 20\%$ throughout the volume [18].

6.1. First measurements using full-sized blocks of $92 \times 92 \times 520 \text{ mm}^3$

Two full-sized blocks of CEREN 25 have been irradiated with a total dose of 10 Gy. The transmission of each of the blocks was compared with that of a third block which had not been irradiated, using a blue LED ($\langle \lambda \rangle = 490 \text{ nm}$). The blocks are instrumented with vacuum photo triodes and the signal is digitised in ADCs.

The relative transmission, T_r , is the ratio of the optical transmission after irradiation to the optical transmission before. Immediately after the irradiation, the relative transmissions of the two blocks were measured to be 29%.

The first block was stored at 0°C for 4 days and after this time the relative transmission increased to 42%. For a further 24 days it remained at room temperature (25°C) and T_r rose to 60%. Following a further 16

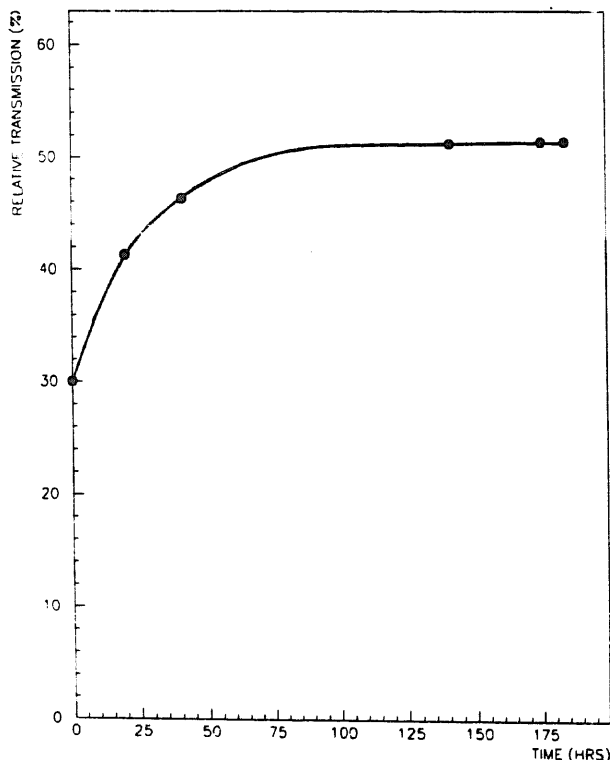


Fig. 26. Relative transmission (see text) for a block of length 520 mm glass as it anneals as a function of time after receiving a dose of 10 Gy. The line through the points is a spline fit drawn to guide the eye.

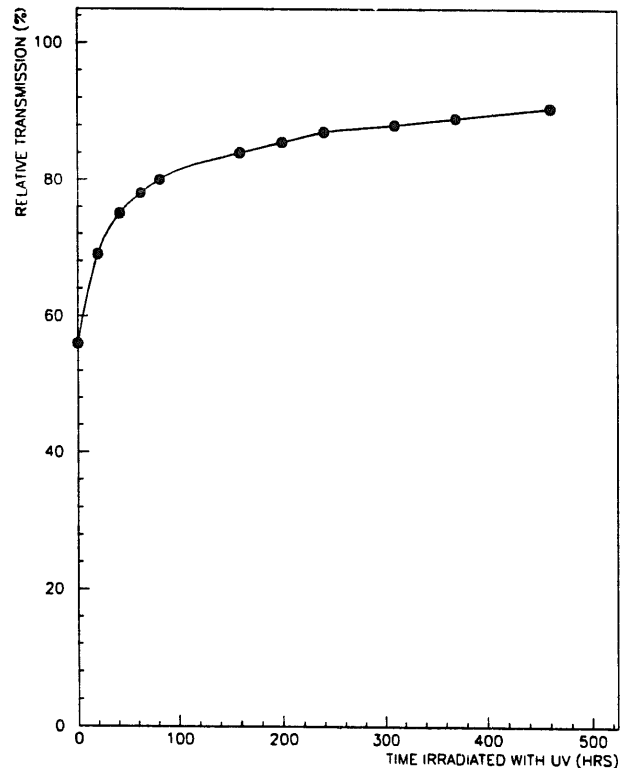


Fig. 27. Relative transmission (see text) after irradiation with UV light, following a dose of 10 Gy and being partially recovered – as shown in fig. 26. The line through the points is a spline fit drawn to guide the eye.

h at 120°C the relative transmission recovered to 98%.

The history of the second block is summarised in figs. 26 and 27. Fig. 26 shows the gradual increase of T_r at room temperature immediately following the irradiation. After this, the block was irradiated with a 125 W Hanova fluorescence lamp and recovered to $T_r = 91\%$ as shown in fig. 27.

The use of UV light and increased temperature to anneal radiation damage in leadglass is a well known procedure [19].

6.2. Second measurements using small samples of glass

A spectrophotometer has been used to measure the effect of irradiation on optical transmission as a function of wavelength using small glass blocks measuring $40 \times 25 \times 10 \text{ mm}^3$. The measurements are made through the 25 mm dimension, approximately one radiation length of CEREN 25. Transmission measurements made in this way always include a loss of light due to reflections from the surfaces of the sample. Correcting for the effects of these reflections gives the "internal transmission".

The advantage of using an intense source of radiation is that measurements can be made as a function of

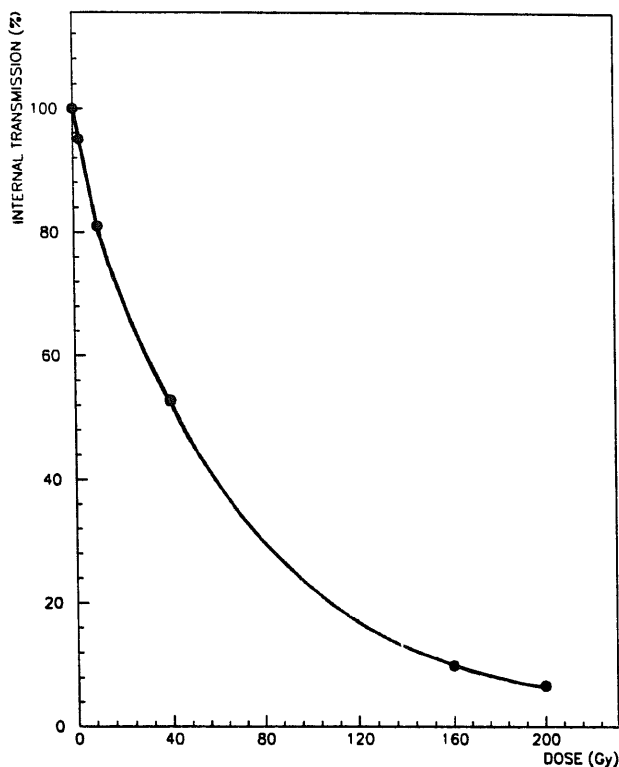


Fig. 28. Internal transmission (see text) through a sample of 25 mm glass as a function of radiation dose. The line through the points is a spline fit drawn to guide the eye.

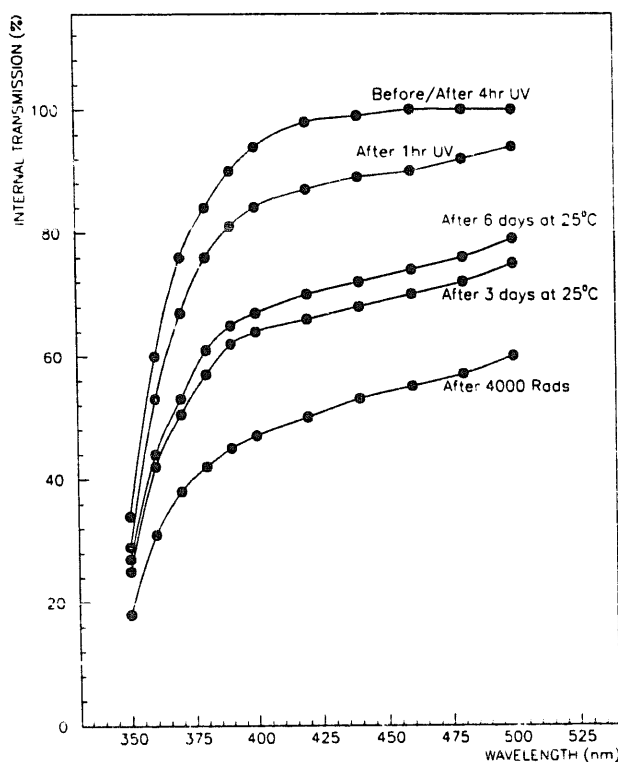


Fig. 29. Internal transmission (see text) through a sample of 25 mm glass as a function of wavelength for various annealing treatments after receiving a total dose of 40 Gy. The lines through the points are spline fits drawn to guide the eye.

applied dose without significant recovery taking place during irradiation. Fig. 28 shows the reduction in transmission with increasing dose measured with light of wavelength $\lambda = 440$ nm. Fig. 29 summarises the full history of a block receiving a total dose of 40 Gy and then being subjected to a number of treatments. The top curve shows the internal transmission measured as a function of spectrophotometer wavelength before receiving radiation. After a dose of 40 Gy the transmission drops by about 50% as shown on the bottom curve. Subsequent curves show the recovery after 3 and 6 days at room temperature, and then 1 and 4 h of UV light. After the combined treatment transmission is recovered. The small block recovers much more quickly than the full-sized block as the UV light can penetrate the entire volume more easily.

7. Conclusions

The OPAL end cap electromagnetic detector was the first calorimeter designed to use leadglass instrumented by vacuum photo triodes, for operation in an intense axial magnetic field. This paper presents a comprehensive set of development measurements which demonstrate the power of the technique.

The equivalent noise of an individual detector is found to be 10 (13) MeV at axial fields of $B = 0.0(0.4)$ T. For energies below 10 GeV, with fields of $B = 0.4$ T, the normalised energy resolution is $\leq 5\%/\sqrt{E}$. The spatial resolution is less than 10 mm for energies ≥ 5 GeV.

Acknowledgement

We thank the Engineering Division of Rutherford Appleton Laboratory for their help in the design, construction and commissioning of the calorimeter counters, for O. Runolfsson and D. Plane from CERN with preparing the test beam equipment and DESY for the loan of the solenoidal magnet.

References

- [1] Technical Proposal - CERN/LEPC/83-4; OPAL Status Report - CERN/LEPC/84-17.
- [2] The OPAL Detector, to be submitted to Nucl. Instr. and Meth.
- [3] The OPAL Detector, to be submitted to Nucl. Instr. and Meth.
- [4] M.D. Rousseau et al., IEEE Trans. Nucl. Sci. NS-30 (1983) 479;
P.W. Jeffreys et al., IEEE Trans. Nucl. Sci. NS-32 (1) (1985);
P.W. Jeffreys et al., submitted to Int. Conf. on High

- Energy Physics, Bari, Italy, Rutherford Report RAL 85-058 (1985).
- [5] The OPAL Detector, to be submitted to Nucl. Instr. and Meth.;
- S. Majewski, F. Charpak, A. Breskin and G. Mikenberg, Nucl. Instr. and Meth. 217 (1983) 265;
- G. Bella et al., Nucl. Instr. and Meth. A252 (1986) 503;
- S. Dado et al., Nucl. Instr. and Meth. A252 (1986) 511;
- G. Mikenberg, Nucl. Instr. and Meth. A265 (1988) 223.
- [6] M. Akrawy et al., to be submitted to Nucl. Instr. and Meth.
- [7] C.W. Fabjan and T. Ludlam, Ann. Rev. Nucl. Part Sci. 32 (1982);
- C.W. Fabjan and R. Wigmans, Energy Measurement of Elementary Particles, CERN-EP/89-64.
- [8] CEREN 25, leadglass manufactured by Corning France, 44 Av. de Valvins, Avon, Cedex 77211, France.
- [9] Philips, RTC La Radiotechnique – Compdec. 130, Ave Ledru-Rollin, PARIS XIe, France.
- [10] R. Stephenson, Rutherford Appleton Laboratory Reports RL 82-082, RL 83-075, RAL 87-019.
- [11] G. Schuler, “96-Channel FASTBUS Charge Integrating ADC – CIAFB F683C – Operation and Manufacture” CERN/EF/4102H/GS/ed (1988).
- [12] W. Kononenko et al., Nucl. Instr. and Meth. 214 (1983) 237.
- [13] Prototype Desy magnet, 2 m long, type C.
- [14] Conical versions have been made which operate with non-axial fields.
- [15] C. Beard et al., to be submitted to Nucl. Instr. and Meth.
- [16] Blocks were manufactured in three lengths: 380, 420, 520 mm, but the tests reported in this paper used 520 mm length blocks.
- [17] P.W. Levy, Amer. Ceramic Soc. 43 (1960) 389.
- [18] Radiation source used was ^{60}Co cells in Hangar 10, Harwell Laboratory, UKAEA, Oxfordshire, OX11 0RA.
- [19] M. Goldberg, P.L. Mattern, K. Lengweiler and P.W. Levy, Nucl. Instr. and Meth. 108 (1973) 119.